

Classification of Benign and Malignant DCE-MRI Breast Tumors by Analyzing the Most Suspect Region

Sylvia Glaßer¹, Uli Niemann¹, Uta Preim², Bernhard Preim¹, Myra Spiliopoulou³

¹Department for Simulation and Graphics, OvG-University Magdeburg

²Department for Radiology, Municipal Hospital Magdeburg

³Knowledge Management and Discovery Lab (KMD), OvG-University Magdeburg
glasser@isg.cs.uni-magdeburg.de

Abstract. Classification of breast tumors solely based on dynamic contrast enhanced magnetic resonance data is a challenge in clinical research. In this paper, we analyze how the most suspect region as group of similarly perfused and spatially connected voxels of a breast tumor contributes to distinguishing between benign and malignant tumors. We use three density-based clustering algorithms to partition a tumor in regions and depict the most suspect one, as delivered by the most stable clustering algorithm. We use the properties of this region for each tumor as input to a classifier. Our preliminary results show that the classifier separates between benign and malignant tumors, and returns predictive attributes that are intuitive to the expert.

1 Introduction

Dynamic contrast enhanced magnetic resonance imaging (DCE-MRI) allows for perfusion characterization of breast tumors. DCE-MRI has high sensitivity but moderate specificity. So, it remains supplemental to conventional X-ray mammography, and is frequently used to confirm the malignancy or benignity of lesions [1]. Malignant breast tumors often lead to neo-angiogenesis with increased tissue permeability and increased number of supporting blood vessels; this is usually reflected in a rapid contrast agent washin and/or washout. Hence, it is typical to define a region of interest (ROI) and compute the ROI's average relative enhancement (RE) over time - the RE curve - for it. From the early RE and the curve's shape, the radiologist assesses the contrast agent washin and washout. Since a breast tumor is as malignant as its most malignant part, the RE curve of this ROI is used to determine the tumor's malignancy. In this study, we partition a ROI into regions that are homogeneous with respect to the RE curves of their voxels, and identify region features that contribute to predict malignancy.

The RE curves of the individual voxels are noisy by nature, so a major challenge lays in grouping them to homogeneous and spatially contiguous regions.

Glaßer et al. propose a region merging method to this purpose [3], which is used in [4] to study the role of tumor heterogeneity in predicting malignancy. Similar to our work is the study of Chen et al. [2], who perform clustering with fuzzy c-means and extract the most characteristic RE curve for the separation between benign and malignant tumors. However, our approach combines the identification of the most suspect region per tumor with the identification of predictive tumor characteristics that hold for multiple tumors.

In this paper, we study a set of 68 breast tumors. For each tumor, we apply multiple density-based clustering algorithms and identify the most suspect region. We extract the properties of this region and show that these properties contribute to distinguishing between benign and malignant tumors. To do so, we perform classification over all tumors, whereby we blend out obvious predictors like tumor size. Our focus relies on clinical research on DCE-MRI tumor enhancement kinetics. In clinical practice, rather, the combination of different image modalities (e.g. X-ray and MRI) with patient-specific attributes (e.g. genetic risk factors) is indispensable for a complete diagnosis.

2 Material and Methods

In this section we describe our medical image data containing the breast tumors, followed by our classification approach based on a tumor’s most suspect region.

2.1 Tumor Data

Our data set comprises 50 patients with 68 breast tumors. 31 tumors proved to be benign and 37 malignant (confirmation was carried out via histopathologic evaluation or by follow up studies after six to nine months). We included only lesions that have been detected in MRI. The data sets were acquired with a 1.0 T open MR scanner and exhibit the parameters: in-plane resolution $\approx 0.67 \times 0.67 mm^2$, matrix $\approx 528 \times 528$, number of slices ≈ 100 , slice gap = $1.5 mm$, number of acquisitions = 5–6 and total acquisition time $\approx 400 sec$. During and immediately after the bolus injection of contrast agent one precontrast and four to five post-contrast images were acquired per series. Since DCE-MRI data exhibit motion artifacts mainly due to thorax expansion through breathing and patient’s movement, motion correction was carried out with MeVisLab (www.mevislab.de), employing the elastic registration developed by Rueckert et al. [5]. Next, the relative enhancement (RE) of a tumor, i.e. the percent aged signal intensity increase, is calculated [1] with $RE = (SI_c - SI)/SI \times 100$. Here, SI is the pre-contrast and SI_c is the post-contrast signal intensity. Each breast tumor was segmented by an experienced radiologist. The segmentation comprises only voxels exhibiting at least 50% RE at the first time step after the early post contrast phase.

2.2 Methods

Our approach consists of two steps: the extraction of the most suspect region for each tumor and the classification process over all tumors (see Fig. 1).

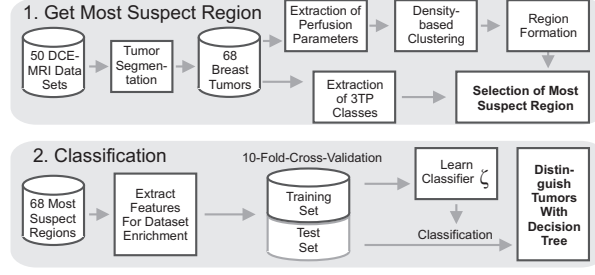


Fig. 1. Schematic overview of the presented approach. First, we determine each tumor’s most suspect region. Second, we learn a classifier to predict malignancy.

Step 1: Extraction of the Most Suspect Region of Each Tumor. We extract the most suspect region by determining descriptive perfusion parameters, three-time-point classes and applying density-based clustering.

The RE plotted over time yields RE curves that allow for the extraction of the descriptive perfusion parameters (see Fig. 2(a)): washin (the steepness of the ascending curve), washout (the steepness of the descending curve), peak enhancement (the maximum RE value), integral (the area under the curve) and time to peak (the time when peak enhancement occurs), which are substitutes for physiological parameters like tumor perfusion and vessel permeability. Since peak enhancement and integral strongly correlate, we exclude peak enhancement from the subsequent analysis.

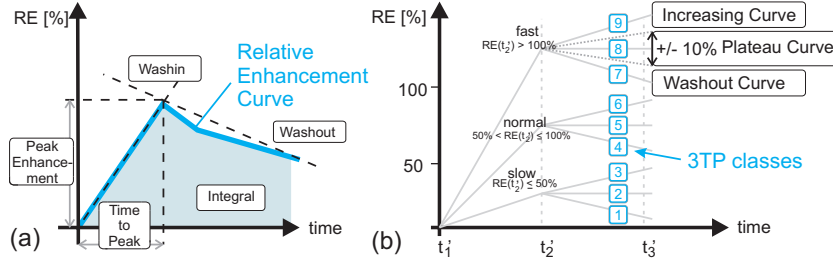


Fig. 2. In (a) a RE curve and its descriptive perfusion parameters are depicted. In (b), the 3TP classes based on RE at t'_1 , t'_2 , and t'_3 are presented.

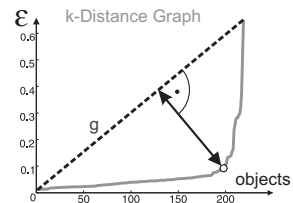
The three-time-point (3TP) method presented by Degani et al. [6] allows for an automatic RE curve classification based on three well chosen time points: t'_1 , the first point in time before the contrast agent injection, t'_2 , 2 min after t'_1 and t'_3 , 4 min after t'_2 . With the 3TP method, a RE change in the interval $\pm 10\%$ in the time between t'_2 and t'_3 will be interpreted as plateau, whereas RE changes higher than 10% and lower than -10% [6] are classified as increasing curve and washout curve, respectively. Since our study contains 5-6 time steps due to different scanning parameters, we assign the third time step to t'_2 and the last time step to t'_3 . The analysis of the initial contrast agent accumulation, i.e. the RE value at t'_2 , which is classified into slow, normal and fast in combination

with the three curve shapes yields nine curve types (see Fig. 2(b)). We compare the results of our clustering algorithms with the 3TP classes.

For the evaluation of the tumor enhancement, voxels with similar RE values should be grouped into regions. To account for irregular and heterogeneous tumor parts, we adapted and applied the following density-based clustering algorithms to all data sets of our study: *Density-based Spatial Clustering of Applications with Noise* (DBSCAN) [7], *Density-Connected Subspace Clustering* (SUBCLU) [8], and *Ordering Points to Identify the Clustering Structure* (OPTICS) [9]. The algorithms separate objects into clusters based on estimated density distributions. They yield clusters with arbitrary shapes, which is important for the underlying medical image data. Objects that do not feature similar objects (i.e. objects with similar parameters) in a given neighbourhood are marked as outliers. That’s a further advantage, since outliers may be caused by a missing inter-voxel-correspondence over time due to motion artifacts.

Next, we employ each voxel’s perfusion parameters and its relative position in the data set as observations. We apply DBSCAN, SUBCLU and OPTICS with the following parameters: the number of minimum points $minPts$ for a cluster is set to 4, 6, and 8. The ϵ -value that determines the size of the neighbourhood depends on the clustering. For DBSCAN and each $minPts$ value, ϵ was automatically determined as suggested in [7]. For SUBCLU, ϵ was extracted from the k-distances graph [7] that maps the distance of an object to its k next neighbours. Our automatic estimation is depicted in Fig. 3. We apply this approach to all four perfusion parameter sets and assign ϵ to the mean of the four estimated values. For OPTICS, we empirically set ϵ to 0.5 and 0.75. With $minPts \in \{4, 6, 8\}$, we get three configurations for DBSCAN and SUBCLU and six configurations for OPTICS yielding 12 clustering results per data set. Spatially connected clusters are maintained by a connected component analysis.

Fig. 3. Determination of ϵ based on the k-distances graph for a given $minPts$ value. The graph maps the distance of an object to its k next neighbours (with $k = minPts$). A well suited ϵ can be detected at a position with increased slope. It is automatically determined by choosing the point with the biggest distance perpendicular to a line g connecting the first and the last point of the graph.



To select the most suspect region, we choose the clustering with the least outliers. Next, we reject all regions that contain less than three voxels. From the remaining regions, we choose the biggest region with an average RE curve of 3TP class 7. If no such region exists, we search for the 3TP class 9, 8, 4, 6, 5, 1, 3, 2 in that order. Although this is a user-defined ranking, we establish this empirical ranking based on definitions of the most malignant tumor enhancement kinetics: a present washout in combination with a strong contrast washin (see Fig. 2(b)).

Step 2: Data Enrichment and Classifier Learning. In the second part, we combine the extracted data to learn a classifier ζ over our 68 breast lesions.

Data enrichment is carried out by including the following attributes of the tumor and its most suspect region: tumor size (in mm^3), number of tumor voxels, percent aged region size, number of region voxels, the similarity measures *Purity* (P), *Jaccard index* (J) and the *F1 score* (F_1) based on the comparison of our clustering and the 3TP-based division (we extracted and include values per tumor, per region and per outlier cluster), the region’s mean perfusion parameters, the number of region voxels of each of the 3TP classes, the most prominent 3TP class (the 3TP class to which the majority of region voxels belong), the region’s mean RE curve, the RE curve’s 3TP class and the patient’s age.

For our approach, we use the J4.8 classification algorithm of the *Waikato Environment for Knowledge Analysis* (Weka) library - a Java software library that encompasses algorithms for data analysis and predictive modelling [10]. J4.8 is based on the C4.5 decision tree classification [11]. It performs 10-fold cross validation and requires at least two instances (two tumors) for each tree leaf. We worked iteratively, reducing the features under consideration and aiming to avoid features that are obviously predictive (such as tumor size), so that the predictive power of other features is highlighted. As a result, we came up with the classifier ζ that was learned on 18 of the original ca. 40 features.

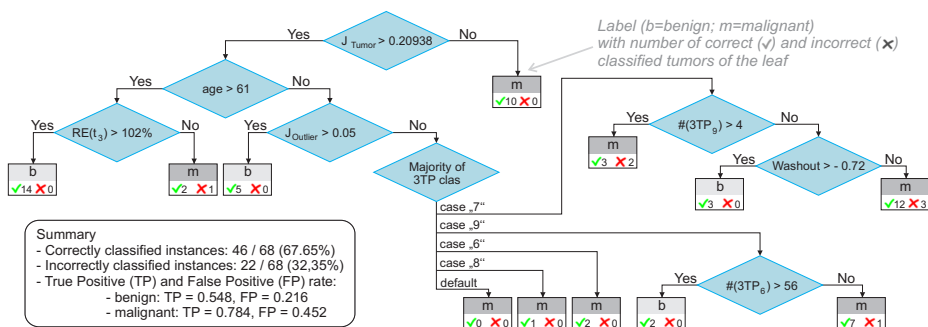


Fig. 4. Learned decision tree: the attributes at the upper part of the tree are the most important ones.

3 Results

We learned a decision tree (see Fig. 4) that employs eight of the 18 features and classifies 46 of the 68 lesions correctly. Features closer to the root of the tree are more important than those at lower levels, because the former help in splitting a larger set of tumors. We can see that the most important attributes are the heterogeneity of the tumor, as identified by the clustering algorithm (represented by J_{Tumor} and $J_{Outlier}$) and the age of the patient. The most prominent 3TP class, the number of voxels in the 3TP class 9 ($\#(3TP_9)$) and 6 ($\#(3TP_6)$), the contrast agent washin ($RE(t_3)$), and washout are also important.

4 Discussion

We presented a new method that combines within-tumor clustering and tumor classification to predict tumor malignancy, and we reported on our preliminary results on a data set with 68 breast tumors. Our first results indicate that the identification of the most suspect region with clustering and the exploitation of this region's features in classification are promising steps in tumor separation. The low sensitivity of our results must be attributed to the specific tumor type, for which it is difficult to distinguish between benignity and malignancy. In the future, we want to deepen and expand our findings in several directions. We intend to use 5-fold cross-validation and more rigid statistics on the 68-tumor data set, since it is very small for training. A further challenge arises from correlated tumors; which come from the same patient. We intend to apply dedicated methods for such instances within a bigger study in the future.

Acknowledgements. This work was supported by the DFG projects SPP 1335 "Scalable Visual Analytics" and SP 572/11-1 "IMPRINT: Incremental Mining for Perennial Object".

References

1. Kuhl CK. The Current Status of Breast MR Imaging, Part I. *Radiology*. 2007;244(2):356–78.
2. Chen W, Giger ML, Bick U, Newstead GM. Automatic identification and classification of characteristic kinetic curves of breast lesions on DCE-MRI. *Medical Physics*. 2006;33(8):2878–87.
3. Glaßer S, Preim U, Tönnies K, Preim B. A visual analytics approach to diagnosis of breast DCE-MRI data. *Computers and Graphics*. 2010;34(5):602 – 611.
4. Preim U, Glaßer S, Preim B, Fischbach F, Rieke J. Computer-aided diagnosis in breast DCE-MRI – Quantification of the heterogeneity of breast lesions. *European Journal of Radiology*. 2012;81(7):1532 – 1538.
5. D Rueckert, L Sonoda, C Hayes and et al . Nonrigid Registration Using Free-Form Deformations: Application to Breast MR Images. *IEEE Trans Med Imaging*. 1999;18(8):712–21.
6. H Degani, V Gusus, D Weinstein and et al . Mapping pathophysiological features of breast tumors by MRI at high spatial resolution. *Nat Med*. 1997;3:780–782.
7. Ester M, Kriegel HP, Sander J, Xu X. A Density-Based Algorithm for Discovering Clusters in Large Spatial Databases with Noise. In: *Proc. of Knowledge Discovery and Data Mining (KDD-96)*; 1996. p. 226–31.
8. Kailing K, Kriegel HP, Kröger P. Density-Connected Subspace Clustering for High-Dimensional Data. In: *Proc. of SIAM Conference on Data Mining*; 2004. p. 246–57.
9. Ankerst M, Breunig MM, Kriegel HP, Sander J. OPTICS: Ordering Points To Identify the Clustering Structure. In: *Proc. of ACM SIGMOD Conference on Management of Data*; 1999. p. 49–60.
10. Holmes G, Donkin A, Witten IH. WEKA: a machine learning workbench. In: *Intelligent Information Systems, 1994. Proceedings of the 1994 Second Australian and New Zealand Conference on*; 1994. p. 357 –361.
11. Quinlan JR. *C4.5: Programs for Machine Learning*. Morgan Kaufmann Publishers; 1993.